Combustion and Flame 197 (2018) 265–275

Contents lists available at ScienceDirect

Combustion and Flame

journal homepage: www.elsevier.com/locate/combustflame

On the application of tabulated dynamic adaptive chemistry in ethylene-fueled supersonic combustion

Kun Wu[a,b], Francesco Contino[c], Wei Yao[a,b,*], Xuejun Fan[a,b,*]

[a] State Key Laboratory of High Temperature Gas Dynamics, Institute of Mechanics, Chinese Academy of Sciences, Beijing 100190, People's Republic of China
[b] School of Engineering Science, University of Chinese Academy of Sciences, Beijing 100049, People's Republic of China
[c] Department of Mechanical Engineering, BURN Joint Research Group, Vrije Universiteit Brussel, Brussels, Belgium

ARTICLE INFO

Article history:
Received 24 January 2018
Revised 14 August 2018
Accepted 19 August 2018
Available online 7 September 2018

Keywords:
Tabulated dynamic adaptive chemistry
Skeletal mechanism
Supersonic combustion
Ethylene
Large Eddy Simulation

ABSTRACT

The demands for extending the limiting operation conditions and enhancing the combustion efficiency of scramjets raise new challenges to the research of reliable robust and controllable flame stabilization in supersonic flows. In the present study, Large Eddy Simulation of flame stabilization in a realistic supersonic combustor, employing the tabulation of dynamic adaptive chemistry (TDAC) method were conducted, in comparisons with other relevant chemistry treatment methods, i.e., dynamic adaptive chemistry (DAC), global skeletal mechanism, and detailed mechanism. The wall pressures, the pseudo one-dimensional metrics, combustor global performance and flame structures are all well reproduced by the DAC/TDAC methods compared with the experimental measurements and the benchmark predictions by the detailed mechanism, while the global skeletal mechanism fails to predict the flame stabilization characteristics. The reason for the discrepancy induced by the skeletal mechanism in the flame stabilization simulation was further illustrated through reaction path analyses. Regarding the computational efficiency, the DAC method shows high efficiency for complex reaction systems, with an almost linear increasing speedup factor with the increase of species number. The TDAC method almost doubly further improves the DAC efficiency. The DAC/TDAC methods show great potential of alleviating the huge computational cost while improving the chemistry fidelity for supersonic combustion especially for flame stabilization modeling.

1. Introduction

Hypersonic air-birthing propulsion systems capable of sustained operation in flight have received renewed research interest during the past decade [1]. Although considerable achievements have been made in understanding the flow physics in scramjet combustors [2], there still remains significant challenges including efficient mixing and stabilized combustion within limited flow residence time. More importantly, with regard to the extension of the operating envelops and enhancement of combustion efficiency, robust flame stabilization was proved to be one of the most intractable challenges. Three different flame stabilization modes in hydrogen fueled dual-mode scramjet were first observed by Micka and Driscoll [3] via flame luminosity experimentally. More comprehensive experiments by Yuan et al. [4] using time-resolved CH* chemiluminescence found four distinct modes in an ethylene-fueled supersonic combustor in which a weak combustion mode is absent in Micak and Driscoll. Wang et al. [2] summarized the state-of-the art about the fundamental problems and recent advances regarding cavity-stabilized scramjet combustor but the lack of comprehensive experimental measurements renders this challenge still unsolved.

However, due to the prohibitive cost of ground test, the difficulties in measuring reacting flow quantities in supersonic flow as well as the complexity of the aerothermodynamics, high-fidelity numerical simulation is not only complementary but is absolutely necessary for understanding and then optimizing the supersonic combustion in scramjets [5,6]. To achieve accurate predictions on the essential physical and chemical properties of the turbulent reacting flow, great efforts have been devoted to the development of high-resolution numerical schemes [7] and turbulent–combustion interaction models [8–10] for supersonic combustion simulation, whereas the importance of the comprehensive chemical mechanism is prominently overlooked. In consideration of this, Wu et al. [11] thoroughly analyzed the influence of chemistry mechanisms in faithfully reproduction the flame stabilization mode in the strut injection scramjet engine. They also realized that various elementary reactions control the flame stabilization mechanism in different reaction zones. In addition, the deficiency of the skeletal mechanism in well reproducing the flame stabilization structure in an

* Corresponding authors at: State Key Laboratory of High Temperature Gas Dynamics, Institute of Mechanics, Chinese Academy of Sciences, Beijing 100190, People's Republic of China.
E-mail addresses: weiyao@imech.ac.cn (W. Yao), xfan@imech.ac.cn (X. Fan).

https://doi.org/10.1016/j.combustflame.2018.08.012
0010-2180/

Nomenclature

Symbols

p	pressure
ρ	density
T	temperature
Y_k	mass fraction of species k
c_k	mole concentration of species k
dQ	heat release rate
$\dot{\omega}$	chemical source term
υ	kinematic viscosity
υ_t	turbulent viscosity
υ_{eff}	effective kinematic viscosity
ε	turbulence dissipation rate
S_{ij}	strain rate tensor
τ_c	characteristic time scale of chemical reaction
τ_m	characteristic time scale of turbulent mixing
κ	reacting volume fraction in PaSR model
Cp	constant pressure specific heat
L	characteristic length of the combustor
H	height of the combustor
t_f	flow through time, $t_f = L/U_\infty$
ψ^q	query composition vector $\psi^q = \{p, T, Y_1, Y_2, \ldots Y_N\}$
ψ_a^q	query composition vector with active species
$\boldsymbol{R}$	reaction mapping
$\mathbf{R}^I$	linearized reaction mapping
ϕ	equivalence ratio
N_{sp}	number of active species
N_{cell}	number of computational cells
η_p	total pressure loss
η_c	global combustion efficiency
dA	incremental area projection in the streamwise direction
ε_{DAC}	threshold value for DAC module
ε_{ISAT}	threshold value for ISAT module
τ_{ing}	ignition delay time
δ_{ing}	relative error of ignition delay time
S_u	laminar flame speed
δ_{su}	relative error of laminar flame speed
Ma	Mach number

sub- and super-scripts

∞	physical properties of the air inflow
^	normalized form of the corresponding physical quantity
$-$	spatial filtering
$\sim$	favre filtering

Abbreviations

DAC	dynamic adaptive chemistry method
ISAT	in-situ adaptive tabulation method
TDAC	tabulation of dynamic adaptive chemistry method
ODE	ordinary differential equation
EOA	ellipsoid of accuracy
DRGEP	directed relation graph with error propagation
DI	direct integration

ethylene-fueled model scramjet was elaborated by comparing with experimental data and results obtained with detail mechanism in Wu et al. [12]. After reviewed plentiful available simulated scenarios, Gonzalez-Juez et al. [6] speculated that an appropriate chemical mechanism is more important, if no remarkable improvement in the treatment of turbulent–combustion interaction can be anticipated.

Improving the accuracy of the chemical mechanisms while minimizing their sizes are both required for the numerical modeling. Usually, adopting reduced or skeletal mechanisms in turbulent combustion modeling is a tradeoff to the formidable computational cost especially in hydrocarbon-fueled propulsion systems [13]. For instance, Potturi and Edwards [14] utilized a 22-species reduced ethylene mechanism in a cavity-stabilized scramjet engine, while Zettervall et al. [15] used a skeletal mechanism of 19 species with 57 reversible reactions to mimic the kerosene combustion chemistry in a multi-burner annular aero-engine combustor. Therefore, exploit the accuracy of the comprehensive chemical mechanism, based on the concept of multiple sets of chemical mechanisms for different reaction zones and different reaction stages, dynamic adaptive chemistry (DAC) method [16] provides a promising approach to retain the mechanism accuracy while minimizing its size spatiotemporally.

In this work, the main objective is to illustrate and analyses the seamless process of utilizing DAC method in supersonic combustion simulation while enhance its efficiency through coupling of the mechanism reduction method with the tabulation algorithm. This strategy, also called tabulation of dynamic adaptive chemistry (TDAC), overcomes the two sources of computational overhead in simulations, i.e. number of cells and chemical species. In the present study, the TDAC method of Contino et al. [17–20] is briefly introduced before the descriptions of the experimental case and the numerical details. The DAC/TDAC methods are firstly applied in simulating auto-ignition and one-dimensional laminar flame propagation to validate their accuracy and efficiency against the direct integration. Then supersonic combustion modelings employing different chemistry treatment methods, i.e., DAC, TDAC and global skeletal mechanism, are compared with those by the detailed mechanism, to further verify their capabilities in flame stabilization prediction.

2. Tabulation of dynamic adaptive chemistry methodology

The computational cost required by reactive flow simulation depends on both the number of grid cells and the complexity of the fuel oxidation mechanisms. Under the framework of direct integration, the total times to solve the system of species evolving equations are proportional to the number of cells. The size of fuel oxidation mechanism determines the workload of the stiff nonlinear solver to integrate the ordinary differential equation (ODE) system. Reduction of computational efforts for these two aspects is achieved by the TDAC method [17] which is briefly illustrated in Fig. 1. The TDAC method is composed of two elementary layers: a tabulation layer and a mechanism reduction layer.

The tabulation layer employs the in situ adaptive tabulation (ISAT) method [21]. During the integration of the species-evolving ODE system over the current time-step, a query composition vector ψ^q is firstly provided to the tabulation layer. The ISAT module will try to retrieve a previously stored result of reaction mapping $\mathbf{R}(\psi^0)$ within the local error threshold ε_{ISAT} and linearly estimates the current reaction mapping as $\mathbf{R}^I(\psi^0)$. If the query is not retrievable within the current ellipsoid of accuracy (EOA), direct integration of the stiff ODE system will be applied and the binary tabulation tree will be expanded by adding a new leaf or growing the current leaf depending on whether the local error exceeds the ε_{ISAT}. The pressure as a status variable is also stored in the ISAT table since the constant pressure assumption is no longer valid for transient supersonic flows with high compressibility. Although similar to the treatment in the internal combustion engine simulation [17], the setup is much more challenging. In the previous engine simulations, pressure changed widely over the entire simulation but without dramatic change within the computational domain, mostly because it was homogeneous charge compression ignition. In su-

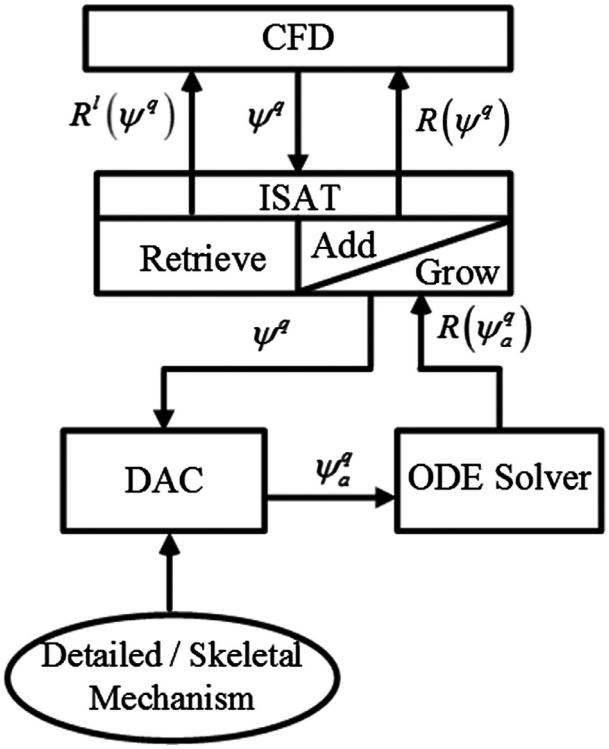

Fig. 1. Coupling algorithm of the in situ adaptive tabulation and adaptive dynamic chemistry in the reacting flow simulation.

personic flows, discontinuity induced by shock waves in the domain is much stronger and more complex to handle for ISAT.

The mechanism reduction module will be activated if the retrieval is impossible. However, instead of generating a global-valid skeletal mechanism for the whole-field reacting statuses, only the information of local thermochemical condition is used to generate a local-valid skeletal mechanism. Since the skeletal mechanism is updated at different reaction stages, e.g., ignition, steady combustion, and extinction, the mechanism can be kept accurately yet small since only the most relevant elementary reactions are retained.

The current mechanism reduction is conducted by directed relation graph with error propagation (DRGEP) algorithm [22], which determines the linking strength of a target specie to the user-defined search initiating set of species while considering the error damping process in the reaction network. The DRGEP method finally extracts a set of active species and their associated elementary reactions based on the local thermochemical states and the error threshold ε_{DAC}. To maintain the consistency during the mechanism switch, the ODE associated with those disabled species are not solved, whereas their concentrations are still considered when involved in the three-body and pressure-dependent reactions. The previous applications of DRGEP-based DAC [19,23] have proved the high efficiency yet adequate accuracy through the synergy of tabulation and dynamic mechanism reduction scheme.

3. Computational specifications

3.1. Experiment description

The supersonic combustion experiment to be studied was conducted by Situ et al. [24] in a directly connected pipe test rig. As schematized in Fig. 2, the quasi two-dimensional combustor is 1100 mm long with a rectangular inlet of 65 mm in height and 40 mm in width. The mixing section occupies 370 mm in length

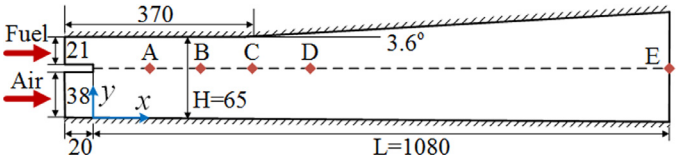

Fig. 2. Schematic of the combustor (unit in mm) with $\hat{x}_A = 0.1$, $\hat{x}_B = 0.2$, $\hat{x}_C = 0.3$, $\hat{x}_D = 0.4$, $\hat{x}_E = 1.0$.

and is followed by a 3.6° unilateral expansion section till the combustor exit. The vitiated air at Mach number (Ma) 2.15 is supplied by a hydrogen-based heater, whereas its oxygen concentration recovers to that of the standard air with makeup oxygen. The resulting composition of the vitiated air was determined by the amount of hydrogen consumed and oxygen replenished to reach 1700 K stagnation temperature at stagnation pressure of 0.0977 MPa.

The fuel stream is fed by the hot products of kerosene/air combustion at Ma = 1.25 from an upstream subsonic combustor. Due to the infeasibility for the on-site measurement of the hot product's composition, it is therefore determined by a simplified chemistry model [24]. Gaseous ethylene was first used as a surrogate intended to represent the products of the thermal-cracked kerosene after initial endothermic reactions [25]. Then, the composition was calculated based on a one-step global reaction to match the combustion efficiency derived from the measured stagnation temperature and pressure at the exit of the upstream subsonic combustor. Both the air and fuel streams were injected axially into the supersonic combustor split by a 6-mm-high plate. Wall pressure was measured by 23 pressure taps on the lower wall and 13 taps on the upper wall. The experimental conditions including the specific compositions of the fuel and the vitiated air streams are summarized in Table 1.

3.2. Numerical details

In this section, the numerical method and related physical models used in the present Large Eddy Simulation (LES) are briefly described. More details can be found in our previous study [11]. The spatially filtered governing equations for mass, momentum, species, and energy are solved. Following the thermal perfect gas assumption, the thermodynamic data are looked up from the NIST-JANAF database [26]. The viscosity is obtained by Sutherland's law, and the thermal and mass diffusivities are calculated by assuming constant Prandtl and Schmidt number. The mixture-averaged diffusive coefficients are calculated using the modified Wilke's law [27].

To close the filtered equations, the subgrid scale viscosity is modeled by the one-equation kinetic energy model [28], in which a transport equation of subgrid kinetic energy is solved. The filtered reaction rates, taking into account the turbulence–chemistry interaction, are modeled using a heterogeneous multi-scale subgrid combustion model named partially stirred reactor model (PaSR) [29]. In the PaSR model, the reacting volume fraction κ is determined by the characteristic time scales of chemical reaction (τ_c) and micro-mixing (τ_m) as $\kappa = \tau_c/(\tau_c + \tau_m)$. The micro-mixing time scale is defined as $\tau_m = (\upsilon_{eff}/\varepsilon)^{1/2}$, in which dissipation rate is obtained by $\varepsilon = 2\upsilon_{eff}|\tilde{S}_{ij}|^2$ while $\upsilon_{eff} = \upsilon_t + \upsilon$. The chemical time scale should be representative of the overall chemical reaction and, although many options are available [30], it is estimated here as the ratio of the summation of species concentrations to that of the forward production rate, $\tau_c = \sum_{k=1}^{NS} c_k / \sum_{k=1}^{NS} \dot{\omega}_k^+$. Consequently, the filtered reaction rate is defined as $\overline{\dot{\omega}(p, \mathrm{T}, Y_i)} = \kappa\overline{\dot{\omega}}(\bar{p}, \tilde{T}, \tilde{Y}_i)$, in which $\overline{\dot{\omega}}(\bar{p}, \tilde{T}, \tilde{Y}_i)$ is the reaction rate based on the filtered physical quantities while κ is used to account for the influence of turbulence on the chemical reactions. The accuracy and reliability of PaSR model have been extensively adopted in supersonic combustion

Table 1
Modeling configurations.

Parameter	P (MPa)	Ma	T (K)	Y_{N2}	Y_{O2}	Y_{C2H4}	Y_{H2O}	Y_{CO2}
Air	0.0977	2.15	491.9	0.7150	0.2330	0.0	0.0520	0
Fuel	0.1731	1.25	1771.9	0.6067	0.0103	0.1059	0.1566	0.1205

modelings [31–35] especially in flame stabilization mode investigations [11,36] which substantiates its applicability in the present study.

Simulations were carried out by using an in-house solver, astroFoam, developed in the OpenFoam framework [37]. The time-integration is performed using the second-order Crank–Nicholson scheme [38]. The convective fluxes are reconstructed using the second-order TVD (total variation diminishing) scheme, while the diffusion fluxes are reconstructed by the central scheme. The resulting algorithm is second-order accurate in both space and time, and the equations are solved with a maximum Courant number restriction of 0.3.

3.3. Chemistry treatment methods

To illustrate the effect of different chemistry treatments, including DAC, TDAC, and global skeletal and detailed mechanisms were utilized in the subsequent simulations. The DAC and TDAC method were previously elaborated in Section 2. The detailed 57-species/269-reactions UCSD mechanism [39] of ethylene-air combustion which has been comprehensively validated in scramjet relevant conditions [12] is taken as the benchmark case (denoted as Detail, hereinafter). The global skeletal mechanism consisting of 30 species and 143 reactions which was delicately developed for scramjet simulations based on the UCSD mechanism is also employed (represented as Skeletal). This global skeletal mechanism was developed using DRGEP mechanism reduction method which is consistent with the present DRGEP-based DAC method, and it has also been extensively validated regarding ignition delay and laminar flame speed in Wu et al. [12].

3.4. Computational implementation

The computational model is depicted in Fig. 2, where the streamwise and transverse coordinates $\hat{x}$ and $\hat{y}$ are normalized, respectively, by the combustor length L and height H. In view of its quasi two-dimensional layout, the computational model spans one twentieth of the width (2 mm) of the combustor in the Z direction. The grid is comprised of block-structured hexahedral cells clustering around the shear layer originating from the splitter. Since the flame locates in the reacting shear layer, it was resolved by 61 transverse grids to accurately capture the turbulent mixing and subsequent reaction. The mean and maximum grid size in the mixing zone are 0.2 mm and 0.35 mm, respectively. The upper and lower combustor walls are treated as slip condition to mitigate the inhibitive grid resolution near the wall, which is unaffordable for the case employing the detailed mechanism. Grid convergence study for the same combustor layout based on 0.14, 0.28 and 0.36 million cells has been conducted previously [12], which has been extended to the prediction of velocity profiles at different streamwise locations as included in the supporting materials. In the systematic grid convergence analysis, the medium grid (0.28 million) shows good agreement with the finer one (0.36 million) and will be used in the present study as a tradeoff between accuracy and computational cost.

Direchlet boundary conditions were imposed to all variables on the combustor inlet except the velocity, which was specified as the superposition of its mean value and sinusoidal perturbation with 5% of its magnitude. Zero-gradient boundary condition

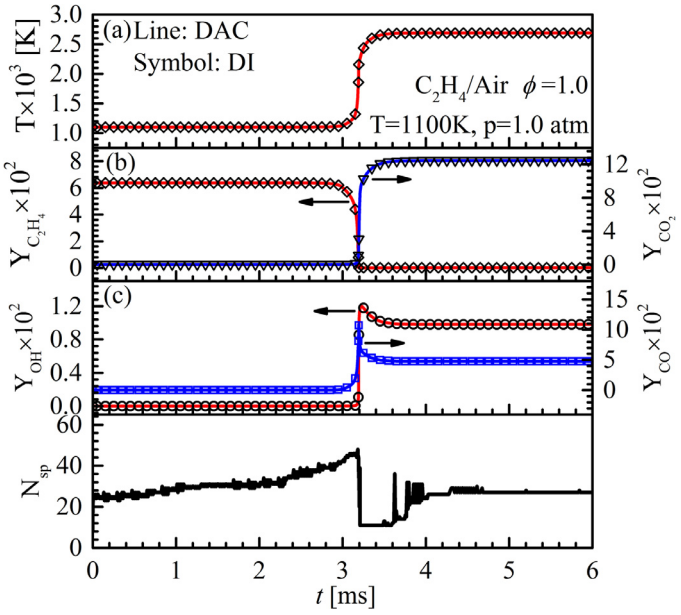

Fig. 3. Time evolution of (a) temperature, (b) mass fraction of C_2H_4, (c) mass fraction of OH, and (d) number of active species in the ethylene/air auto-ignition predicted by DAC and DI based on the UCSD mechanism.

is applied to the supersonic outlet at the combustor exit. To facilitate the following discussion, the pressure, temperature, and velocity are scaled by the air stream values as $\hat{p} = p/p_\infty$, $\hat{T} = T/T_\infty$, $\hat{U} = U/U_\infty$. The scaling of heat release rate dQ takes the form of $d\hat{Q} = dQ/C_pT$, where C_p and T are the local constant-pressure specific heat and temperature, respectively. The flow-through time approximates $t_f = L/U_\infty \approx 1.2$ ms. A typical run takes $12t_f$, with $4t_f$ to reach the statistically steady state and $8t_f$ for the statistical data collection.

4. Validation of TDAC configurations in canonical problems

4.1. Auto-ignition demonstration

The DAC part of the TDAC method was first validated in auto-ignition calculations in constant pressure batch reactor, where stoichiometric ethylene-air mixture reacts at a constant pressure of 1.0 atm and an initial temperature of 1100 K. The search initiating set of species is chosen to be the fuel species (C_2H_4), O_2 and N_2 in the mechanism reduction as in the development of skeletal mechanism in Wu et al. [12], Niemeyer et al. [40] and Sun et al. [41]. The tolerance in the DAC method is set to 10^{-3} according to the convergence study presented in Appendix A1 which is also adopted in the previous study [18].

In Fig. 3a, the temperature profile closely follows the direct integration calculation, especially the onset location of the temperature. In addition, the results by the DAC for the mass fractions of C_2H_4, CO_2, and active radicals OH and CO also show very good agreements in Fig. 3b and c. Fig. 3(d) presents the time variation of active species number (N_{sp}), which firstly increases with the increase of mixture reactivity and then drops abruptly after the ig-

Table 2
Speed-up factors of DAC in auto-ignition tests.

Fuel	Mechanism	Species	Reactions	Speed-up factor
Ethylene	UCSD [39]	57	269	3.8
Ethylene	Laskin [42]	75	529	4.2
Ethylene	USCII [43]	111	784	7.2
Iso-octane	Curran et al. [44]	874	3796	37.5
Kerosene	Dagaut et al. [45]	2185	8217	441.3

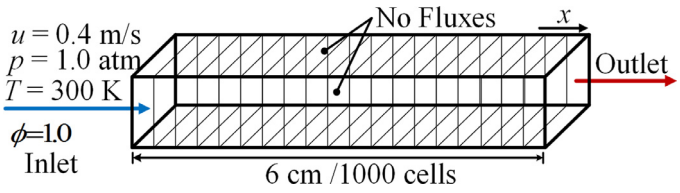

Fig. 4. Computational setup for the 1-D ethylene/air flame propagation test.

nition. It should be noted that proper selection of target species for the mechanism phase is an important consideration. Liang et al. [16] analyzed the influence of target species selection for homogeneous charge compression ignition (HCCI) combustion of *n*-heptane, indicating that proper selection of target species for the mechanism reduction is important, but this topic merits further study for general applications. Although different from the search initiating species set in Contino et al. [17], the auto-ignition test verified the validity of the present selection. Additional analysis on the influence of the search initiating set in auto-ignition calculation and also the subsequent scramjet combustor modeling is presented in the supporting materials.

Table 2 shows the speed-up factors defined as the ratio between average CPU times by direct integration (DI) and DAC method. To analyze the effect of the mechanism size, three ethylene mechanisms [39,42,43] with increasing number of species have been used. The contribution of DAC is demonstrated by the use of various mechanisms, where the efficiency of the DAC method increases almost linearly with the number of species. The DAC was also used in auto-ignition calculations involving iso-octane [44] and kerosene [45] mechanisms, where 37.5- and 441.3-fold speed-up are attained, respectively, which indicates the great potential of DAC in scramjet or rocket simulations.

4.2. Laminar flame propagation test

As a fundamental element in combustion, accurate prediction of the laminar flame is of great importance in reacting flow simulations. Besides, the performance of including pressure as a status variable in the ISAT module is not fully validated yet. Therefore, the TDAC method is further verified in one-dimensional freely flame propagation problem. As shown in Fig. 4, stoichiometric ethylene/air mixture enters from the left end of the domain at given velocity with the temperature $T_0 = 300$ K. Inside the domain, the fuel is consumed by the combustion leading to a flame propagating against the fresh gas. The static pressure has been kept constant over the whole domain of $p = 1.0$ atm. The 6-cm-long computational domain is equidistantly discretized by 1000 grids. The error threshold for the ISAT module is 10^{-4} following the previous studies [18,19]. Comprehensive convergence studies on the threshold values of DAC and ISAT for laminar flame speed simulations were elaborated in Appendix A2 which further justify the present configurations.

From Fig. 5, the calculated temperature and species mass fractions by DAC and TDAC both compare well with those by direct integration. The result calculated using ISAT is also shown in Fig. 5 and the good agreement further verified the present ISAT configuration. The achieved speedup factors are listed in Table 3 as a function of the chemical mechanism size and the number of grid cells. The speed-up factor increases with the increase of the grid cells since the times of chemical integration vary approximately proportional to the cell number. The relatively low efficiency of the ISAT method compared with those by Pope [21] and Lu et al. [46] may attribute to the flow inhomogeneity and the wider range of thermochemical statuses in the current modeled cases. In the TDAC method coupling ISAT with DAC, the speedup factor even exceeds the product of their own individual speedup factors, and a maximum speedup factor of 8.7 has been achieved.

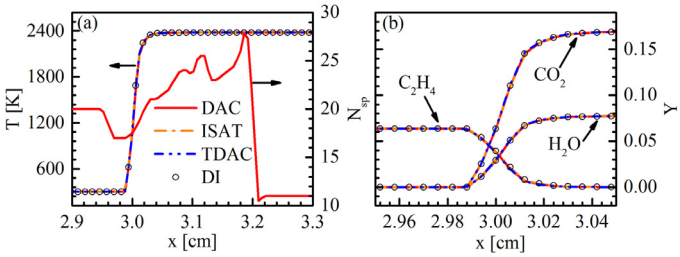

Fig. 5. Spatial distribution of (a) T and active DAC species number and (b) mass fractions of C_2H_4, CO_2, and H_2O in the ethylene/air flame propagation test under atmospheric pressure and temperature of 298 K using different chemistry treatment methods.

Table 3
Speed-up factor obtained for laminr flame calculations of stoichiometric ethylene-air mixture at atmopheric pressure and inflow temperature 300 K.

Species	Reactions	Method	N_{cell}				
			250	500	1000	2000	5000
57	269	DAC	1.7	1.7	1.7	1.7	1.9
		ISAT	1.2	1.2	1.4	1.7	1.9
		TDAC	2.0	3.0	4.2	5.0	7.3
75	529	DAC	2.1	2.1	2.1	2.1	2.2
		ISAT	1.2	1.2	1.4	1.7	2.0
		TDAC	3.1	3.2	4.7	5.3	7.8
111	784	DAC	2.3	2.3	2.3	2.3	2.5
		ISAT	1.2	1.2	1.4	1.7	1.9
		TDAC	4.0	4.3	5.5	6.6	8.7

5. TDAC augmented supersonic combustion modeling

5.1. Experimental validation

After thorough comparisons in canonical problems, different chemistry treatment methods will be compared in the LES modeling of a realistic supersonic combustor. In consideration of the uncertainties in determining the compositions in both air and fuel streams, a benchmark employing detailed mechanism was conducted to provide the utmost details of chemical kinetics. In Fig. 6, the time-averaged pressure contours predicted by different chemistry treatment methods are presented. The DAC and TDAC predictions show qualitatively identical wave structures with the prediction by the detailed mechanism. The fuel and air streams impinge upon each other forming upper expansion wave and lower oblique shock wave. The reflected expansion wave and shock wave interact at location $\hat{x} \approx 0.115$ which is well captured by the three chemistry treatment methods compared with the prediction by the detailed mechanism. The second impinging point of the reflected shock wave on the upper wall, as denoted by the marker line, is accurately predicted by the DAC and the TDAC methods, but shifts slightly upstream to $\hat{x} \approx 0.282$ in the global skeletal mechanism's prediction.

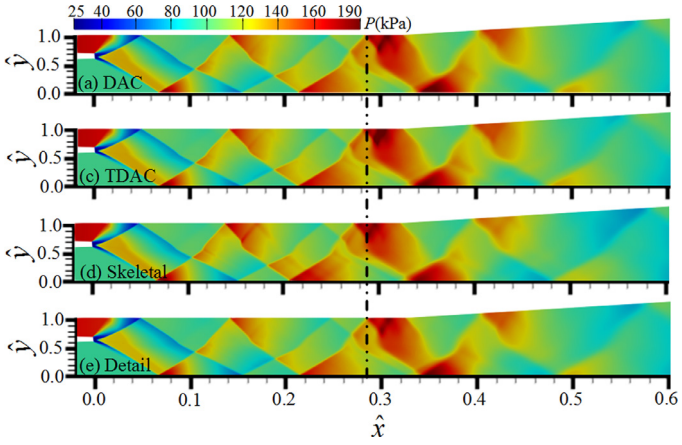

Fig. 6. Time-averaged pressure contours predicted by (a) DAC, (b) TDAC, (c) the global skeletal mechanism and (d) the detailed mechanism.

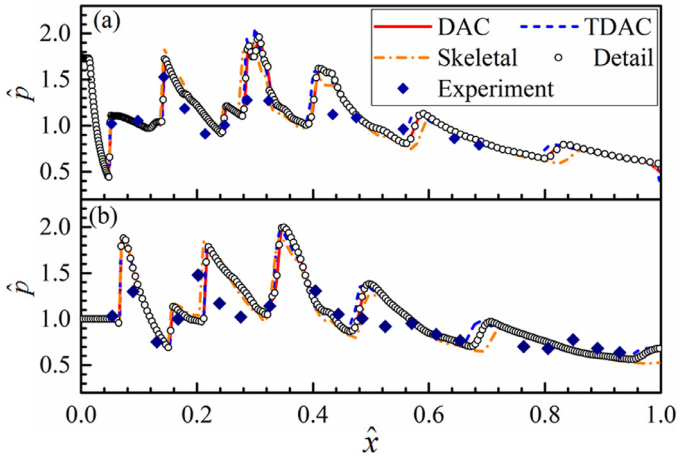

Fig. 7. Pressure distributions on both the (a) upper and (b) lower combustor walls predicted by different chemistry treatment methods.

Quantitatively comparisons of combustor wall pressure are shown in Fig. 7. Compared with the experiment, all the four methods produce good agreements, especially for the locations of the turning points. Due to the sparse measurements, the experimental data just serves as a global validation of the present numerical method and setups, and the subsequent discussions will mainly rely on results from the detailed mechanism. To be specific, the very small discrepancy is measured by a relative error $\varepsilon_{\varphi,\ method}$ to quantitatively assess the predictions by different methods,

$$\varepsilon_{\varphi,\ method} = \frac{1}{K}\sum_{i=1}^{K} |\varphi_{i,method} - \varphi_{i,detail}|/\varphi_{i,detail} \tag{1}$$

where K is the number of sampling points on the combustor wall, the subscript φ and *method* denote the variable to be assessed and the chemistry treatment method used. As can be seen in Fig. 7, the best agreement is achieved by the DAC method, with $\varepsilon_{p,DAC} = 0.26\%$ and 0.29% on the upper and lower walls, respectively. The TDAC method produces slightly larger derivations in the downstream, with $\varepsilon_{p,\ TDAC}$=1.09% and 0.41% for the upper and lower walls. In Fig. 7(a), the global skeletal mechanism method predicts a slightly earlier pressure rise at $\hat{x} \approx 0.282$, corresponding to the upstream shifting of the reflected shock wave there as in Fig. 6c. Relatively larger discrepancies exist in predicting other impinging points, e.g., the one at $\hat{x} \approx 0.415$. The global skeletal mechanism method shows the largest overall discrepancies, i.e., $\varepsilon_{p,\ skeletal} = 4.08\%$ and 3.70% on the upper and lower walls, respectively.

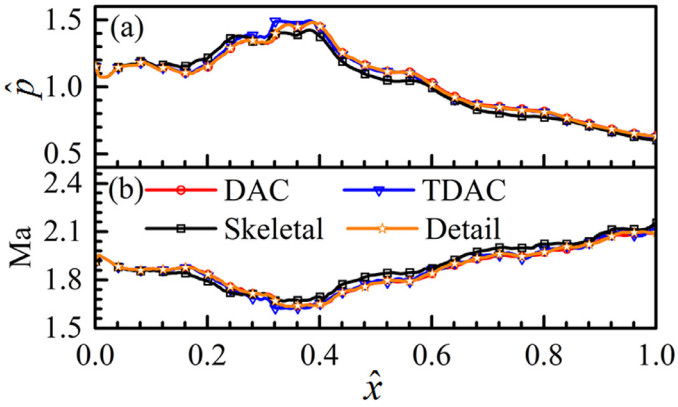

Fig. 8. Pseudo one-dimensional streamwise profiles of (a) pressure and (b) Ma predicted by different chemistry treatment methods.

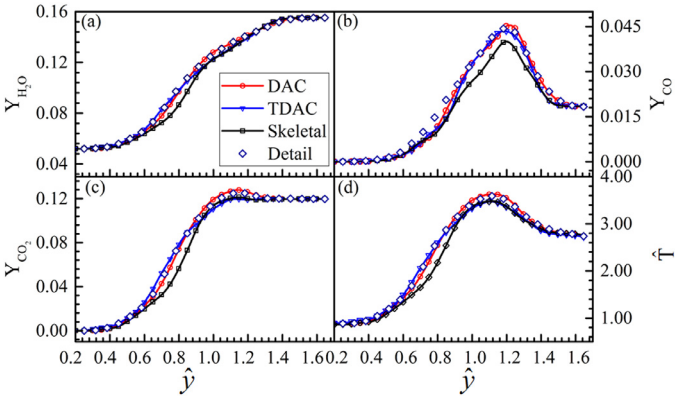

Fig. 9. Time-averaged mass fractions of (a) H_2O, (b) CO, (c) CO_2 and (d) temperature on the combustor exit predicted by different chemistry treatment methods.

5.2. Combustor global performance evaluation

The pseudo one-dimensional analysis is regards as a reliable yet efficient tool in global performance evaluation in scramjet experiment and design [47]. Therefore, the pseudo one-dimensional pressure and Ma profiles are calculated as the mass-weighted average on cross-sections at different streamwise locations. As shown in Fig. 8, the profiles predicted by the DAC method closely coincide with those predicted by the detailed mechanism, with small relative errors being 0.92% and 0.33% for pressure and Ma, respectively. The TDAC predictions also shows good agreement with $\varepsilon_{p,DAC} = 1.06\%$ and $\varepsilon_{Ma,DAC} = 1.28\%$, albeit relatively larger deviation at $\hat{x} \approx 0.3$ for the pressure profile. On the contrast, the global skeletal mechanism method shows evident discrepancies in both the Ma and pressure profiles, with $\varepsilon_{p,DAC} = 3.51\%$ and $\varepsilon_{Ma,DAC} = 3.76\%$.

Thermochemical status characterized by the static temperature and mass fractions of key species including CO, CO_2, and H_2O at the combustor exit is probed and shown in Fig. 9. The profiles predicted by the DAC method again coincide well with those predicted by the detailed mechanism for all the metrics presented. The TDAC method also accurately reproduces all the profiles with slightly larger discrepancies. However, the global skeletal mechanism method considerably underpredicts the temperature, the mass fractions of CO_2 and H_2O in range $0.6 \le \hat{y} \le 0.9$, and is especially worsen in reproducing the peak of CO mass fraction in Fig. 9b.

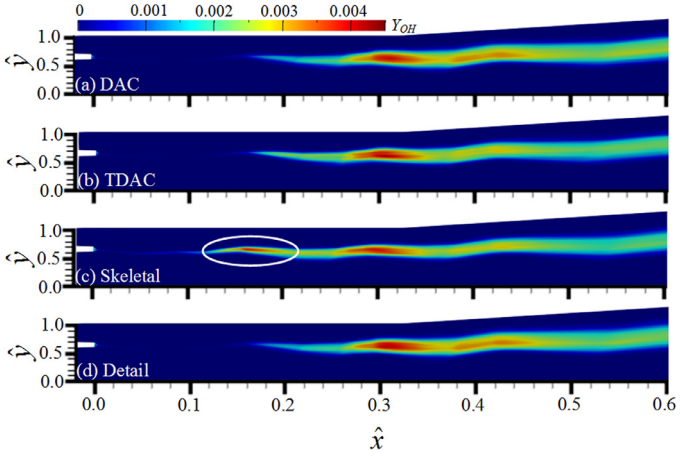

Fig. 10. Time-averaged OH radical contours predicted by (a) DAC, (b) TDAC, (c) the global skeletal mechanism and (d) the detailed mechanism.

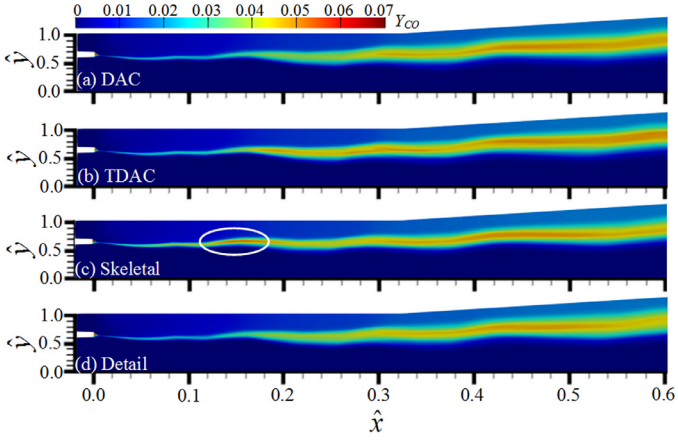

Fig. 11. Time-averaged CO radical contours predicted by (a) DAC, (b) TDAC, (c) the global skeletal mechanism and (d) the detailed mechanism.

The combustion efficiency and total pressure loss can be calculated using the sampled data at the combustor exit. The total pressure loss is calculated according to Baurel et al. [48] as,

$$\eta_t = 1 - \frac{\int \rho u p_{0,exit} dA}{\int \rho u p_{0,inlet} dA} \tag{2}$$

where ρ, u and dA are the density, the streamwise velocity component, and the incremental area projection in the streamwise direction. $p_{0,\,exit}$ and $p_{0,\,inlet}$ are the total pressures at the combustor exit and inlet, respectively. The total pressure loss predicted by the DAC and the TDAC methods are, respectively, 42.3% and 43.1%, which are very close to the prediction of 42.5% by the detailed mechanism. The total pressure loss calculated by the global skeletal mechanism method is slightly higher as 45.0% but is still rather close to the prediction by the detailed mechanism. The combustion efficiency is calculated directly from the heat release rate as [12],

$$\eta_c = \frac{\int \rho u dQ dA}{\sum_{inlet} \left(\dot{m}_{fuel} Y_{C2H4}\right) q_c} \tag{3}$$

in which dQ denotes the heat release rate, $\dot{m}_{fuel}$ is the mass flow rate of the fuel, Y_{C2H4} is the mass fraction of ethylene in the fuel stream at the combustor inlet, and q_c is the heat of combustion of ethylene under standard condition. The overall combustion efficiencies are 57.6% for the DAC method, 58.1% for the TDAC method, and 58.2% for the global skeletal method, which are all close to 57.8% predicted by the detailed mechanism. Based on the above comparisons, the differences between various chemistry treatments are negligible small due to the integral nature of the global combustion performance metrics. This further substantiates the feasibility of utilizing skeletal mechanism in scramjet global performance evaluation as has been discussed in our previous work [12].

5.3. Flame stabilization prediction

The flame structures characterized by the distributions of OH radicals is shown in Fig. 10. It can be seen that the DAC and TDAC methods reproduce qualitatively similar reaction zones as that predicted by the detailed mechanism. The reaction zone resides in the shear layer between air and fuel stream emanating from $\hat{x} \approx 0.15$ in the prediction by the detailed mechanism. However, the reaction zone reproduced by the global skeletal mechanism shows remarkable difference between that by the detailed one, in which an evident reactive pocket emerges accompanied by a local extreme at $\hat{x} \approx 0.15$. Similar deviation exists in the CO distributions

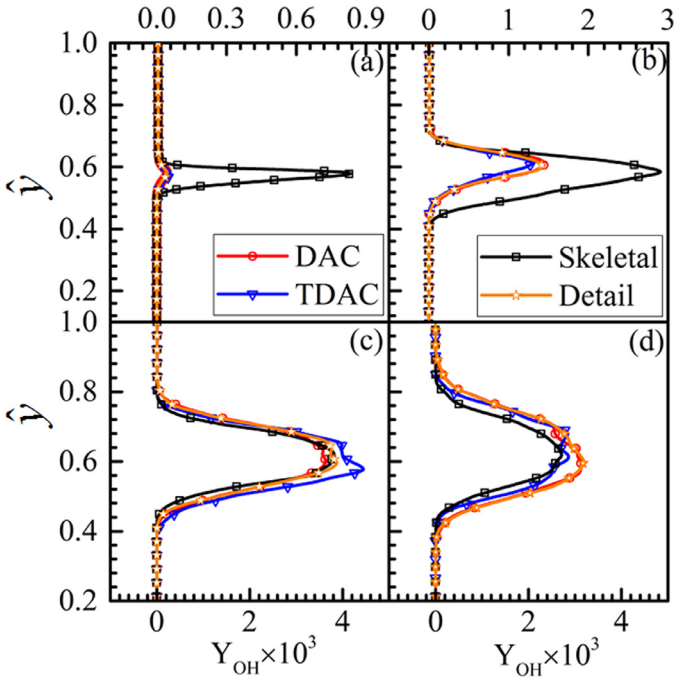

Fig. 12. Time-averaged OH mass fractions distribution predicted by different chemistry treatment methods at streamwise locations (a) A, (b) B, (c) C and (d) D.

between the predictions by the global skeletal mechanism and the detailed mechanism in Fig. 11, where CO becomes relatively rich at $\hat{x} \approx 0.12$.

To quantify the differences in the flame stabilization structure, the streamwise evolution of time-averaged Y_{OH} and Y_{CO} were probed at four streamwise locations: $\hat{x}_A = 0.1$, $\hat{x}_B = 0.2$, $\hat{x}_C = 0.3$ and $\hat{x}_D = 0.4$ along the combustor. In Fig. 12, at the most upstream location (Fig. 12a), the detailed mechanism, DAC and TDAC methods predict negligible amount of OH production, but the global skeletal mechanism method remarkably overpredicts the mass fraction of OH. At location B, the skeletal mechanism treatment still evidently overpredicts the Y_{OH} and shows a much wider reaction zone. On the contrary, DAC and TDAC methods again achieve good agreements with the detailed mechanism. The discrepancy in the predictions for CO is similar, i.e., the global skeletal method overpredicts the mass fraction of CO at locations A and B, while the DAC and TDAC methods give fairly good predictions compared

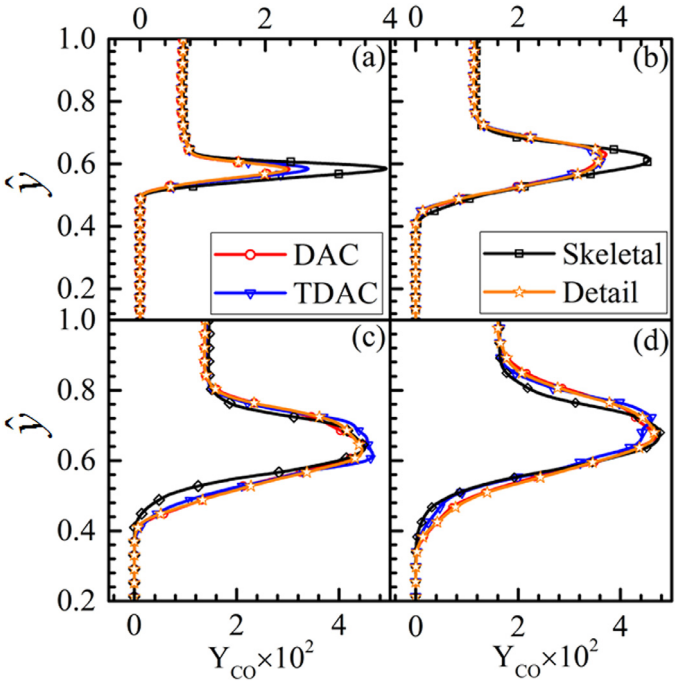

Fig. 13. Time-averaged CO mass fractions predicted by different chemistry treatment methods at locations (a) A, (b) B, (c) C, and (d) D.

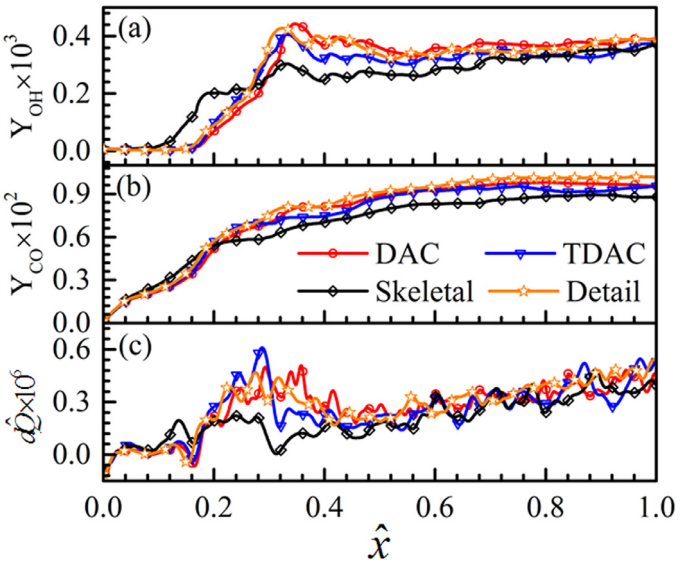

Fig. 14. Pseudo streamwise profiles of time-averaged (a) mass fractions of OH and (b) CO, and (c) heat release rate predicted by different chemistry treatment methods.

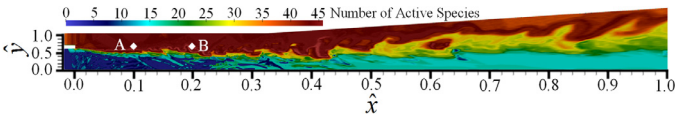

Fig. 15. Distribution of the number of active DAC species at $t=6t_f$.

with the predictions by the detailed mechanism. At downstream locations C and D, the differences between all the predictions diminish considerably.

Fig. 14 shows the pseudo one-dimensional profiles for the mass fractions of OH, CO radicals and the heat release rate, which are calculated by mass-flux-weighted averaging on different cross-

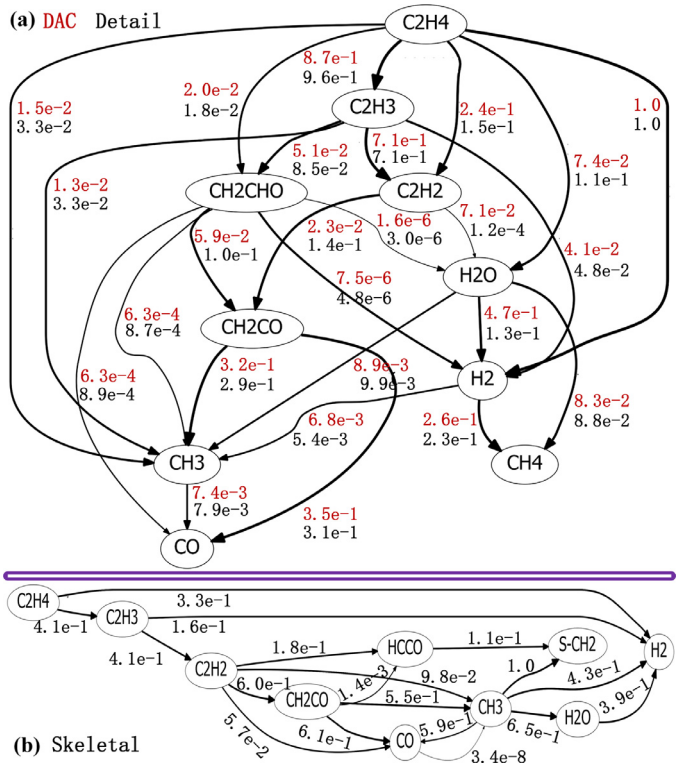

Fig. 16. Reaction path analysis at location A and $t=6t_f$ for (a) DAC and the detail mechanism, and (b) the global skeletal mechanism.

sections perpendicular to the streamwise direction. The DAC and TDAC methods well reproduce the tendency and the magnitude of Y_{OH} compared with the prediction by the detail mechanism. The global skeletal mechanism method predicts a much earlier rise up at $\hat{x}\approx0.06$ and then significantly underpredicts the magnitude between $\hat{x}=0.24$ and 0.65 for the Y_{OH} profile. Regarding the CO profile, the DAC and TDAC predictions show good agreements with the prediction by the detailed mechanism, whereas the global skeletal mechanism method underpredicts its magnitude from $\hat{x}=0.2$ to the combustor exit. The heat release distribution which is the main concern in the thermal protection in scramjet engine is also compared in Fig. 14c. It can be seen that the heat release rate manifests more intense fluctuations compared with the radical profiles. Although relatively large discrepancies are observed in the DAC and TDAC predictions, their general trends coincide with the prediction by the detailed mechanism and the turning point at $\hat{x}\approx0.16$ is accurately captured. However, the prediction by the global skeletal mechanism is in poorer agreement with that by the detailed mechanism from $\hat{x}$=0.12 to 0.4 while misses the main peak at $\hat{x}\approx0.24$.

5.4. Computational efficiency comparison

To analyze the efficiency of the DAC method, the instantaneous contour of active species number at $t=6t_f$, i.e., 7.2 ms is presented in Fig. 15. The chemical reaction in the combustor can be roughly divided into several reaction zones according to the number of active species, which reflects different reaction stages. Generally, the pyrolysis stage for the fuel converting into smaller hydrocarbons or radicals, possibly with the help of H and OH radicals, involves many more reactions than the combustion stage [49]. In the upper half part before $\hat{x}=0.4$, pyrolysis reactions take place in the high-temperature fuel rich mixture which involves more than 40 species. On the contrary, in the lower half part before $\hat{x}=0.4$, only

Table 4
Speed-up factors in the supersonic combustion modelings.

	Detail	Skeletal	DAC	TDAC
Information	57S/269R	30S/143R	–	–
Method	–	DRGEP	DRGEP	DRGEP + ISAT
Speedup Factor	1.0	3.85	3.12	5.56

a small number of species are needed to characterize the almost reaction-frozen vitiated air.

Further downstream after $\hat{x} = 0.4$, three stratified layers in the transverse direction can be observed: 1) the upper fuel layer still in pyrolysis, 2) the unreacted lower vitiated air layer, and 3) the intermediate mixed layer with intense combustion reactions involving 25–30 species. The DAC method dynamically update the local reaction pool to only include the most relevant reactions, thus minimizing the chemistry solving cost. As compared in Table 4, the DAC method achieves a speed-up factor of 3.12, which is only slightly lower than the global skeletal mechanism method of 3.85. However, the efficiency of DAC can be further improved through coupling with the tabulation method, e.g., the ISAT method used in this study, to attain a higher value of 5.56.

5.5. Chemical kinetic analysis of DAC

Throughout the above comparisons, the DAC predictions show excellent agreements with the predictions by the detailed mechanism for wall pressure, combustor global performance, and flame stabilization reproduction while the predictions by the global skeletal mechanism exhibit remarkable differences especially in the reaction zone prediction. To scrutinize the underlying reason for these discrepancies, reaction path analyses for the DAC procedure at two representative locations A and B were conducted. The simulations are calculated in zero-dimensional homogeneous adiabatic reactor under the same thermochemical conditions probed, respectively, at locations A and B in the supersonic combustion flow at $t = 6t_f$. Since the chemical mechanism used in the DAC method is varying tempospatially, the local valid mechanism was extracted at the same time.

To facilitate the comparison, the time of 10 K initial increase of the temperature was selected for the reaction path analysis for all mechanisms. The number of the displayed species in reaction pathways was limited to 10 according to ranking of the maximum rate of depletion of all species. The main reaction pathway for the detailed mechanism at location A is depicted in Fig. 16(a). It can be seen that through the interactions with H, O and OH, C_2H_4 was converted to C_2H_3 and CH_2CHO radicals initially. Another source of CH_2CHO production was the reactions of C_2H_3 radical with O_2 and OH radicals via $C_2H_3 + O_2 = CH_2CHO + O$ and $C_2H_3 + OH = CH_2CHO + H_2$. The C_2H_3 radicals can also undergo the H-abstraction reactions leading to C_2H_2 formation. Subsequent reactions of CH_2CHO lead to the formation of CH_2CO and C_1 radical species while the C_2H_2 is mainly consumed in the oxidation reaction chains: $C_2H_2 \rightarrow CH_2CO \rightarrow CH_3 \rightarrow CO$. It should be noted that, in the detailed mechanism, the double-bound-braking reaction $C_2H_4 + O \rightarrow CH_3 + HCO$ and the direct conversion of C_2H_4 to C_2H_2 are also important sources of ethylene consumption.

As shown in Fig. 16a, at location A, the DAC method retains all the important reaction paths in the detailed mechanism, despite some derivations in the net reaction fluxes. However, in reaction pathway of the global skeletal mechanism as shown in Fig. 16b, the main ethylene consumption is limited to the H-abstraction process in the path of $C_2H_4 \rightarrow C_2H_3 \rightarrow C_2H_2 \rightarrow CO$ and the formation of CH_2CO via $C_2H_2 + OH = CH_2CO + H$. Moreover, the important intermediate radical CH_2CHO in Fig. 16 (a) is not presented in that

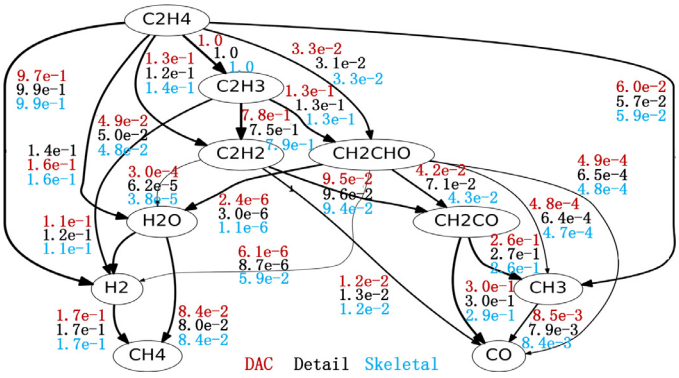

Fig. 17. Reaction path analysis at location B and $t = 6t_f$ for DAC, the detailed mechanism, and the global skeletal mechanism.

of the skeletal one which inevitably changed the overall reaction path. Consequently, large variations are observed in the OH and CO predictions in Figs. 12a and 13a, as the result of the totally different reaction paths. This also suggests that the global skeletal mechanism is not enough to accurately describe all the thermochemical statuses, and multiple sets of skeletal mechanisms for different reaction zones are necessary to improve the accuracy while minimizing the chemistry solving cost. The current validations of the DAC/TDAC methods show their great potential of alleviating the huge computational cost while improving the chemistry fidelity for supersonic combustion modelings.

At location B, the main oxidation reaction pathways of the detailed mechanism are similar to that at location A. Regarding other two chemistry treatment methods as shown in Fig. 17, the most important reaction paths in DAC method, global skeletal mechanism and detailed mechanism at location B are the same, with only minor differences in the net reaction flux. This indicates that the current DAC method has imposed with a relative conservative error threshold to restore the original detailed mechanism in the downstream locations. Therefore, yet more speed-up space left for the DAC method through optimizing the local error threshold(s) during the mechanism reduction which merits further studies.

6. Concluding remarks

TDAC method augmented high-fidelity simulation of supersonic combustion in scramjet concerning the intricate flame stabilization was realized in the present study. The DAC and TDAC methods were first validated in zero-dimensional autoignition and one-dimensional flame propagating problems, where satisfying accuracy and efficiency were obtained in the present configuration. In the realistic scramjet simulation, three different chemistry treatments namely DAC, TDAC and skeletal mechanism were validated against the experiment and the predictions by the detailed mechanism, all of which show good agreement in the combustor wall pressure measurements and engine global performance. In these global or integral metrics predictions, the DAC and TDAC outperform the skeletal mechanism method quantitatively while the TDAC method gain more advantages in efficiency.

For the flame stabilization analysis, the predictions by the global skeletal mechanism show significant discrepancies with those predicted by the detailed mechanism, while the DAC/TDAC methods well predict the heat release rate and the mass fractions of important intermediate radicals (e.g., OH and CO). The reaction path analysis shows that the main reaction paths in the global skeletal mechanism significantly differ from those in the detailed mechanism, while the DAC method retains all the important reac-

tion paths of the detailed mechanism. This suggests that the global skeletal mechanism is not enough to accurately describe all the thermochemical statuses.

In the supersonic combustion modeling, through dynamically updating the local reaction pool to only include the most relevant reactions, the DAC method shows a comparable efficiency with the skeletal mechanism method and the TDAC method almost doubly further improves the DAC efficiency. Therefore, the TDAC method is proven to be a high fidelity yet efficient method in supersonic combustion simulation especially in intricate combustion phenomena while the skeletal mechanism is more suitable in engine's global performance evaluation.

Acknowledgment

The present study is financially supported by the Training Program of the Major Research Plan of the National Natural Science Foundation of China (Grant no. 91641110) and National Natural Science Foundation of China (Grant no. 11502270). The authors are grateful to National Supercomputer Center in Tianjin for providing the computational resource.

Supplementary materials

Supplementary material associated with this article can be found, in the online version, at doi:10.1016/j.combustflame.2018.08.012.

Appendix

A1. Effect of the ε_{DAC} on the autoignition delay calculation

Effect of the threshold ε_{DAC} has been evaluated for stoichiometric ethylene-air mixture at initial temperature 1100 K and atmospheric pressure using UCSD mechanism. Table A1 shows that the agreement between ignition delay times calculated using DAC and detailed mechanism improves as ε_{DAC} decreases from 10^{-2} to 10^{-4}, after which the discrepancy becomes indiscernible. This improvement should be attributed to the increase in active species retained in the reduced mechanism, as shown in Fig. A1. The effects of ε_{DAC} on the number of active species is more appreciable in the pre-ignition stage. In contrast, the number of active species varies between 24 and 27 in the post-ignition stage and seems insensitive to ε_{DAC}.

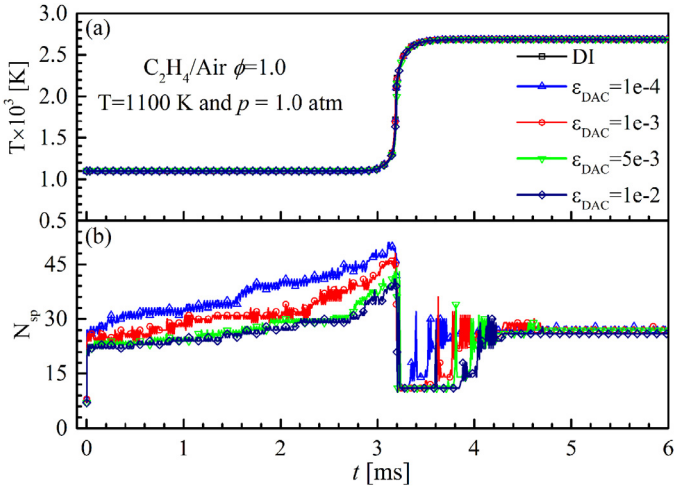

Fig. A1. Convergence study of ε_{DAC} on the autoignition delay time calculations using UCSD ethylene mechanism.

A2. Effect of the ε_{DAC} and ε_{ISAT} on the flame propagation calculation

To quantify the effects of the threshold values on the flame propagation calculation, systematic convergence study was conducted. As shown in Table A2, the relative error in laminar flame speed prediction becomes lager as the increase of ε_{DAC} with only one exception. When ε_{DAC} equals 5×10^{-3}, δ_{Su} slightly decreases compared to the prediction with $\varepsilon_{DAC} = 10^{-3}$ due to the increase in active species (as shown in Fig. A2) which inevitably retards the computational efficiency. The relative error in laminar flame speed induced by ε_{ISAT} is also presented in Table 2. The result indicates that ε_{ISAT} should not exceeds 5×10^{-4} if the relative error is expected to keep within 15%.

Table A1
Convergence study of ε_{DAC} on the autoignition delay time calculations.

ε_{DAC}	0	1×10^{-4}	1×10^{-3}	5×10^{-3}	1×10^{-2}
τ_{ing} [ms]	3.17752	3.17752	3.17751	3.18026	3.18102
δ_{ing}	0	~0	3.1×10^{-6}	8.6×10^{-4}	1.1×10^{-3}
Speed-up factor	1.0	2.1	3.8	4.7	4.9

Notation: τ_{ing} ignition delay time, δ_{ing} relative error of ignition delay time.

Table A2
Convergence study of error threshold for DAC and ISAT modules in flame propagation calculation.

	ε_{DAC}	0	1×10^{-4}	1×10^{-3}	5×10^{-3}	1×10^{-2}
DAC	S_u [cm/s]	70.91	72.40	73.32	72.90	78.43
	δ_{Su}	0	2.1%	3.2%	2.8%	10.6%
	Speed-up factor	1.0	1.3	1.7	1.4	2.6
	ε_{ISAT}	0	1×10^{-5}	1×10^{-4}	5×10^{-4}	1×10^{-3}
ISAT	S_u [cm/s]	70.91	73.28	74.45	79.46	92.19
	δ_{Su}	0	3.34%	4.99%	12.06%	30.01%
	Speed-up factor	1.0	1.2	1.4	1.8	3.7

Notation: S_u laminar flame speed, δ_{Su} relative error of laminar flame speed.

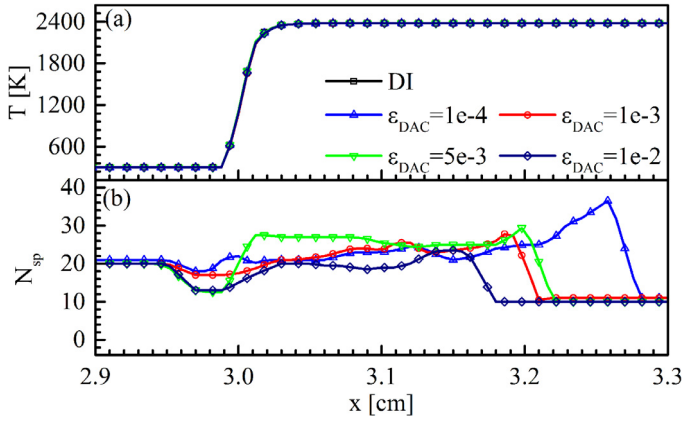

Fig. A2. Convergence study of ε_{DAC} on the laminar flame speed calculations using UCSD ethylene mechanism.

References

[1] M.A. Bolender, B. Dauby, J.A. Muse, D. Adamczak, HIFiRE 6: overview and status update 2014, AIAA Paper, AIAA-2015-3537.

[2] Z. Wang, H. Wang, M. Sun, Review of cavity-stabilized combustion for scramjet applications, Proc. Inst. Mech. Eng. Part G – J. Aerosp. Eng. 228 (2014) 2718–2735.

[3] D.J. Micka, J.F. Driscoll, Combustion characteristics of a dual-mode scramjet combustor with cavity flameholder, Proc. Combust. Inst. 32 (2009) 2397–2404.

[4] Y. Yuan, T. Zhang, W. Yao, X. Fan, P. Zhang, Characterization of flame stabilization modes in an ethylene-fueled supersonic combustor using time-resolved CH* chemiluminescence, Proc. Combust. Inst. 36 (2017) 2919–2925.

[5] J.P. Drummond, Methods for prediction of high-speed reacting flows in aerospace propulsion, AIAA J. 52 (2014) 465–485.

[6] E.D. Gonzalez-Juez, A.R. Kerstein, R. Ranjan, S. Menon, Advances and challenges in modeling high-speed turbulent combustion in propulsion systems, Prog. Energy Combust. Sci. 60 (2017) 26–67.

[7] S. Pirozzoli, Numerical methods for high-speed flows, Annu. Rev. Fluid Mech. 43 (2011) 163–194.

[8] H. Pitsch, Large-eddy simulation of turbulent combustion, Annu. Rev. Fluid Mech. 38 (2006) 453–482.

[9] J.A. Fulton, J.R. Edwards, A. Cutler, J. McDaniel, C. Goyne, Turbulence/chemistry interactions in a ramp-stabilized supersonic hydrogen–air diffusion flame, Combust. Flame 174 (2016) 152–165.

[10] C. Fureby, LES for supersonic combustion, AIAA Paper, AIAA-2012-5979.

[11] K. Wu, P. Zhang, W. Yao, X. Fan, Numerical investigation on flame stabilization in DLR hydrogen supersonic combustor with strut injection, Combust. Sci. Technol. 189 (2017) 2154–2179.

[12] K. Wu, W. Yao, X. Fan, Development and fidelity evaluation of a skeletal ethylene mechanism under scramjet-relevant conditions, Energy Fuels 31 (2017) 14296–14305.

[13] T. Lu, C.K. Law, Toward accommodating realistic fuel chemistry in large-scale computations, Prog. Energy Combust. Sci. 35 (2009) 192–215.

[14] A.S. Potturi, J.R. Edwards, Large-eddy/Reynolds-averaged Navier–Stokes simulation of cavity-stabilized ethylene combustion, Combust. Flame 162 (2015) 1176–1192.

[15] N. Zettervall, E. Fedina, K. Nordin-Bates, E. Heimdal Nilsson, C. Fureby, Combustion LES of a multi-burner annular aeroengine combustor using a skeletal reaction mechanism for jet-a air mixtures, AIAA Paper, AIAA-2015-4020.

[16] L. Liang, J.G. Stevens, J.T. Farrell, A dynamic adaptive chemistry scheme for reactive flow computations, Proc. Combust. Inst. 32 (2009) 527–534.

[17] F. Contino, H. Jeanmart, T. Lucchini, G. D'Errico, Coupling of in situ adaptive tabulation and dynamic adaptive chemistry: an effective method for solving combustion in engine simulations, Proc. Combust. Inst. 33 (2011) 3057–3064.

[18] F. Contino, T. Lucchini, G. D'Errico, C. Duynslaegher, V. Dias, H. Jeanmart, Simulations of advanced combustion modes using detailed chemistry combined with tabulation and mechanism reduction techniques, SAE Int. J. Engines 5 (2012) 185–196.

[19] F. Contino, F. Foucher, P. Dagaut, T. Lucchini, G. D'Errico, C. Mounaïm-Rousselle, Experimental and numerical analysis of nitric oxide effect on the ignition of iso-octane in a single cylinder HCCI engine, Combust. Flame 160 (2013) 1476–1483.

[20] F. Contino, J.-B. Masurier, F. Foucher, T. Lucchini, G. D'Errico, P. Dagaut, CFD simulations using the TDAC method to model iso-octane combustion for a large range of ozone seeding and temperature conditions in a single cylinder HCCI engine, Fuel 137 (2014) 179–184.

[21] S.B. Pope, Computationally efficient implementation of combustion chemistry usingin situadaptive tabulation, Combust. Theory Model. 1 (1997) 41–63.

[22] P. Pepiot desjardins, H. Pitsch, An efficient error-propagation-based reduction method for large chemical kinetic mechanisms, Combust. Flame 154 (2008) 67–81.

[23] Y. Shi, L. Liang, H.-W. Ge, R.D. Reitz, Acceleration of the chemistry solver for modeling DI engine combustion using dynamic adaptive chemistry (DAC) schemes, Combust. Theory Model. 14 (2010) 69–89.

[24] M. Situ, Y. Sun, S. Zhang, C. Wang, Investigation of supersonic combustion of hydrocarbon fuel-riched hot gas in scramjet combustor, AIAA Paper, AIAA-1999-2245.

[25] G. Molvik, J. Bowles, L.O.C. Huynh, Analysis of a hydrocarbon scramjet with augmented preburning, AIAA Paper, AIAA-1992-3425.

[26] M.W. Chase, JANAF thermochemical tables, J. Phys. Chem. Ref. Data 3 (1974) 311–480.

[27] R.B. Bird, W.E. Stewart, E.N. Lightfoot, D.B. Spalding, Transport Phenomena, 2nd ed., John Wiley & Sons, New York, USA, 2002.

[28] A. Yoshizawa, Statistical theory for compressible turbulent shear flows, with the application to subgrid modeling, Phys. Fluids 29 (1986) 2152–2164.

[29] A. Karlsson, Modeling auto-ignition, flame propagation and combustion in non-stationary turbulent sprays, Chalmers University of Technology, 1995.

[30] A. Potturi, J.R. Edwards, Investigation of Subgrid Closure Models for Finite-Rate Scramjet Combustion, AIAA Paper, AIAA-2013-2461.

[31] A.S. Potturi, J.R. Edwards, Hybrid large-Eddy/Reynolds-averaged Navier–Stokes simulations of flow through a model scramjet, AIAA J. 52 (2014) 1417–1429.

[32] C. Fureby, E. Fedina, J. Tegnér, A computational study of supersonic combustion behind a wedge-shaped flameholder, Shock Waves 24 (2014) 41–50.

[33] Y. Moule, V. Sabelnikov, A. Mura, Highly resolved numerical simulation of combustion in supersonic hydrogen–air coflowing jets, Combust. Flame 161 (2014) 2647–2668.

[34] W. Yao, Y. Lu, K. Wu, J. Wang, X. Fan, Modeling analysis of an actively cooled scramjet combustor under different kerosene/air ratios, J. Propuls. Power (2018) 1–17, doi:10.2514/1.b36866.

[35] W. Yao, Y. Yuan, X. Li, J. Wang, K. Wu, X. Fan, Comparative study of elliptic and round scramjet combustors fueled by RP-3, J. Propuls. Power (2017) 1–15, doi:10.2514/1.b36721.

[36] C. Fureby, J. Tegnér, R. Farinaccio, R. Stowe, D. Alexander, A computational study of a dual-mode ramjet combustor with a cavity flameholder, Int. J. Energy Mater. Chem. Propuls. 11 (2012) 487–510.

[37] H.G. Weller, G. Tabor, H. Jasak, C. Fureby, A tensorial approach to CFD using object oriented techniques, Comput. Phys. 12 (1997) 620–631.

[38] M.H. Baba-Ahmadi, G. Tabor, Inlet conditions for LES using mapping and feedback control, Comput. Fluids 38 (2009) 1299–1311.

[39] S.D.M.w.p. "Chemical-kinetic mechanisms for combustion applications", Mechanical and Aerospace Engineering (Combustion Research), University of California at San Diego; (http://combustion.ucsd.edu).

[40] K.E. Niemeyer, C.-J. Sung, M.P. Raju, Skeletal mechanism generation for surrogate fuels using directed relation graph with error propagation and sensitivity analysis, Combust. Flame 157 (2010) 1760–1770.

[41] W. Sun, Z. Chen, X. Gou, Y. Ju, A path flux analysis method for the reduction of detailed chemical kinetic mechanisms, Combust. Flame 157 (2010) 1298–1307.

[42] H. Wang, A. Laskin, A comprehensive kinetic model of ethylene and acetylene oxidation at high temperatures, Progress Report for an AFOSR New World Vista Program, (1998).

[43] X. You, H. Wang, A.V. Joshi, S.G. Davis, A. Laskin, F. Egolfopoulos and C.K. Law, USC mech version II. High-temperature combustion reaction model of H2/CO/C1-C4 compounds; (http://ignis.usc.edu/USC_Mech_II.htm).

[44] H.J. Curran, P. Gaffuri, W.J. Pitz, C.K. Westbrook, A comprehensive modeling study of iso-octane oxidation, Combust. Flame 129 (2002) 253–280.

[45] P. Dagaut, M. Cathonnet, The ignition, oxidation, and combustion of kerosene: a review of experimental and kinetic modeling, Prog. Energy Combust. Sci. 32 (2006) 48–92.

[46] L. Lu, S.R. Lantz, Z. Ren, S.B. Pope, Computationally efficient implementation of combustion chemistry in parallel PDF calculations, J. Comput. Phys. 228 (2009) 5490–5525.

[47] L. Tian, L. Chen, Q. Chen, F. Li, X. Chang, Quasi-one-dimensional multimodes analysis for dual-mode scramjet, J. Propuls. Power 30 (2014) 1559–1567.

[48] R. Baurle, T. Mathur, M. Gruber, K. Jackson, A numerical and experimental investigation of a scramjet combustor for hypersonic missile applications, AIAA Paper, AIAA-1998-3121.

[49] C. Law, A. Makino, T. Lu, On the off-stoichiometric peaking of adiabatic flame temperature, Combust. Flame 145 (2006) 808–819.